

Monte Carlo Simulation of Correlation Measurements of Photon Interrogation of Nuclear Material

November 2006

Prepared by

**Shaun Clarke
Sara A. Pozzi
Enrico Padovani
Thomas J. Downar
Paul Hausladen
John T. Mihalcz
Alan W. Hunt**

DOCUMENT AVAILABILITY

Reports produced after January 1, 1996, are generally available free via the U.S. Department of Energy (DOE) Information Bridge.

Web site <http://www.osti.gov/bridge>

Reports produced before January 1, 1996, may be purchased by members of the public from the following source.

National Technical Information Service
5285 Port Royal Road
Springfield, VA 22161
Telephone 703-605-6000 (1-800-553-6847)
TDD 703-487-4639
Fax 703-605-6900
E-mail info@ntis.gov
Web site <http://www.ntis.gov/support/ordernowabout.htm>

Reports are available to DOE employees, DOE contractors, Energy Technology Data Exchange (ETDE) representatives, and International Nuclear Information System (INIS) representatives from the following source.

Office of Scientific and Technical Information
P.O. Box 62
Oak Ridge, TN 37831
Telephone 865-576-8401
Fax 865-576-5728
E-mail reports@osti.gov
Web site <http://www.osti.gov/contact.html>

This report was prepared as an account of work sponsored by an agency of the United States Government. Neither the United States government nor any agency thereof, nor any of their employees, makes any warranty, express or implied, or assumes any legal liability or responsibility for the accuracy, completeness, or usefulness of any information, apparatus, product, or process disclosed, or represents that its use would not infringe privately owned rights. Reference herein to any specific commercial product, process, or service by trade name, trademark, manufacturer, or otherwise, does not necessarily constitute or imply its endorsement, recommendation, or favoring by the United States Government or any agency thereof. The views and opinions of authors expressed herein do not necessarily state or reflect those of the United States Government or any agency thereof.

Nuclear Science and Technology Division

**MONTE CARLO SIMULATION OF CORRELATION MEASUREMENTS OF
PHOTON INTERROGATION OF NUCLEAR MATERIAL**

S. Clarke,^{*,1} S. A. Pozzi,² E. Padovani,³ T. J. Downar,¹ P. Hausladen²,
J. T. Mihalczo,² and A. W. Hunt⁴

¹*School of Nuclear Engineering, Purdue University, West Lafayette, IN 47907*

²*Oak Ridge National Laboratory, Oak Ridge, TN 37831*

³*Department of Nuclear Engineering, Polytechnic of Milan, Milan, Italy*

⁴*Idaho State University, Pocatello, ID 83209*

Date Published: November 2006

Prepared by
OAK RIDGE NATIONAL LABORATORY
P.O. Box 2008
Oak Ridge, Tennessee 37831-6285
managed by
UT-BATTELLE, LLC
for the
U.S. DEPARTMENT OF ENERGY
under contract DE-AC05-00OR22725

* On research assignment at Oak Ridge National Laboratory.

CONTENTS

	Page
LIST OF FIGURES	v
LIST OF TABLES	vii
ACRONYMS	ix
ABSTRACT	xi
1. INTRODUCTION	1
2. EXISTING IAC EXPERIMENTAL CONFIGURATION AND RESULTS	1
3. COMPARISON OF RESULTS	3
4. PROPOSED IAC EXPERIMENTAL SETUP	6
5. ANALYSIS OF PROPOSED SETUP	7
6. ANALYSIS OF ACCIDENTAL COINCIDENCES	12
7. DISCUSSION AND CONCLUSIONS	16
8. ACKNOWLEDGMENT	16
9. REFERENCES	17
APPENDIX A. MCNPX INPUT FILE	A-3
APPENDIX B. MCNP-POLIMI INPUT FILE FOR EXISTING EXPERIMENTAL GEOMETRY	B-3
APPENDIX C. MCNP-POLIMI INPUT FILE FOR PROPOSED EXPERIMENTAL GEOMETRY	C-3

LIST OF FIGURES

Figure	Page
1. Photonuclear reaction cross sections for uranium-238	1
2. Schematic of the MCNP-PoliMi model of the existing Idaho Accelerator Center experimental setup (not to scale).....	2
3. Idaho Accelerator Center measurement results for bremsstrahlung interrogation of a depleted uranium target	3
4. Comparison of MCNP-PoliMi calculations to experimental data taken by Idaho Accelerator Center for (a) 1.11-m and (b) 2.01-m stop-detector separations.	5
5. MCNP-PoliMi simulation results for the existing experimental setup at 1.11-m stop-detector separation.....	6
6. MCNP-PoliMi simulation results for the existing experimental setup at 1.11-m stop-detector separation.....	6
7. Schematic of the MCNP-PoliMi model of the proposed Idaho Accelerator Center experimental setup (not to scale).....	7
8. MCNP-PoliMi-simulated cross-correlation function for proposed experimental configuration with a depleted uranium target.....	8
9. MCNP-PoliMi-simulated cross-correlation function for proposed experimental configuration with a depleted uranium target.....	8
10. Photonuclear cross sections for three common lead isotopes.....	9
11. MCNP-PoliMi-simulated cross-correlation function for proposed experimental configuration with a lead target.....	10
12. MCNP-PoliMi-simulated cross-correlation function for proposed experimental configuration with a lead target.....	11
13. Comparison of MCNP-PoliMi-simulated cross-correlation functions for depleted uranium and lead targets with a 47-keV detector threshold.....	11
14. Comparison of MCNP-PoliMi-simulated cross-correlation functions for depleted uranium and lead targets with a 500-keV detector threshold.....	12
15. Time of flight for three target materials: highly enriched uranium, depleted uranium, and lead.	13

16.	Time-of-flight distributions for varying numbers of photons per burst for the depleted uranium target.....	14
17.	Distribution of real and accidental coincidences for the depleted uranium target.	14
18.	Distribution of real and accidental coincidences for the lead target.....	15
19.	Distribution of real and accidental coincidences for the highly enriched uranium target.....	15

LIST OF TABLES

Table		Page
1.	Percentage and average energy of the three possible photonuclear reactions occurring in uranium-238 as obtained from MCNPX.....	3
2.	Operational parameters of Idaho Accelerator Center LINAC	12
3.	Number of photonuclear events occurring per source photon in various target materials	13

ACRONYMS

IAC	Idaho Accelerator Center
LINAC	linear accelerator
ORNL	Oak Ridge National Laboratory

ABSTRACT

This report presents the results of Oak Ridge National Laboratory (ORNL) simulations to reproduce time-of-flight data taken at the Idaho Accelerator Center (IAC). The simulations were performed using the ORNL MCNPX/MCNP-PoliMi code system, which calculates the full statistics of the neutron/photon field generated from photonuclear reactions occurring during material interrogation with high-energy photons. The results documented in this report show that ORNL obtained excellent agreement with the measured data for interrogation of a depleted uranium target with 15 MeV endpoint bremsstrahlung photons for two different detector separation distances. Based on these results, ORNL wishes to perform some extended experiments at the IAC; specifically, a second stop detector should be implemented to enable correlation measurements. This configuration has also been simulated and correlation functions obtained for both the standard depleted uranium target as well as a natural lead target, which has a photonuclear neutron-production cross section via a (γ , n) reaction that peaks at approximately the same energy as that for uranium. These reactions also have associated gamma rays and thus can illicit a similar detector response to interrogation of fissile material. However, it has been shown that the lack of multineutron-producing reactions in lead leads to a dramatically different correlated-detector response. The response of benign nuclear materials to interrogation is of interest to applications in homeland security.

1. INTRODUCTION

The content of this report is based on the results and conclusions of simulations made at Oak Ridge National Laboratory (ORNL) for comparison to experimental data taken at the Idaho Accelerator Center (IAC). The IAC data consist of time-of-flight measurements of gammas and neutrons emitted immediately after interrogating a depleted uranium target with 15 MeV endpoint bremsstrahlung photons; the photonuclear cross sections for uranium-238 are shown in Fig. 1 (IAEA Photonuclear Data 2006). The measurements were made using time-correlated plastic scintillation detectors, which are sensitive to both neutrons and gamma rays emitted from the induced photonuclear events within the target.

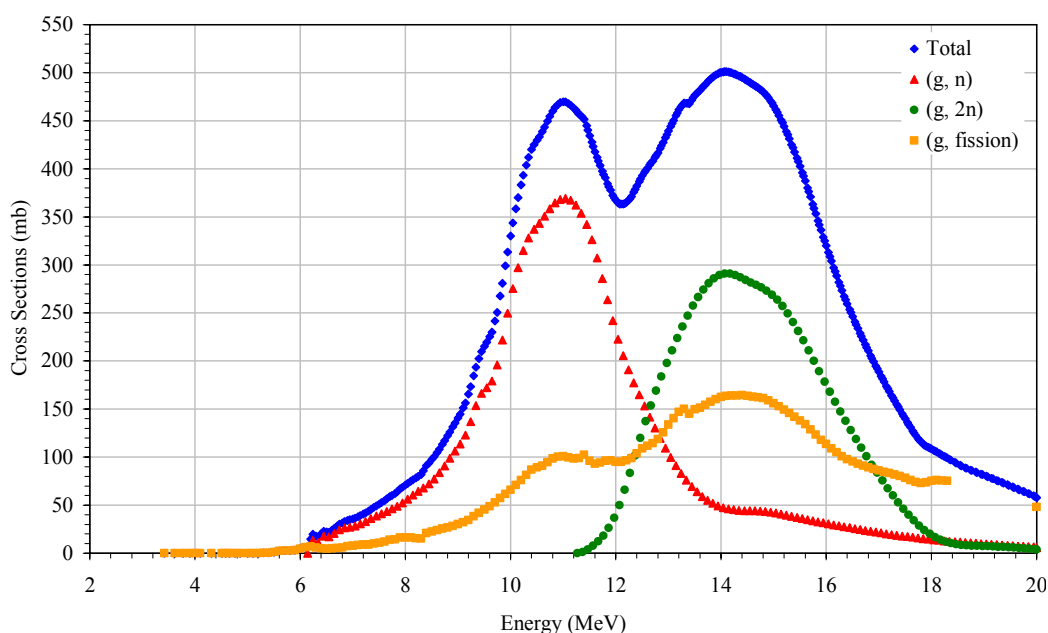


Fig. 1. Photonuclear reaction cross sections for uranium-238.

The secondary goal of this work is to plan some future experiments that would use the IAC facilities. To plan these experiments, it must first be shown that the existing MCNP-PoliMi code system is capable of accurately predicting the photonuclear physics within the target (Pozzi, Padovani, and Marseguerra 2003) Once this has been verified, the MCNP-PoliMi code system can be used to model a proposed experimental system.

2. EXISTING IAC EXPERIMENTAL CONFIGURATION AND RESULTS

Experimental data were taken by the IAC using a 15-MeV endpoint bremsstrahlung source and a depleted uranium target. The source diameter was assumed to be equal to that of the collimator. Correlation measurements were made with two 2-in.-by-2-in. cylindrical plastic scintillation detectors. The detector directly in line with the beam was designated as the start detector; a lead-shielded stop detector was oriented 90° to the

uranium target. An illustration of the experimental setup is shown in Fig. 2.

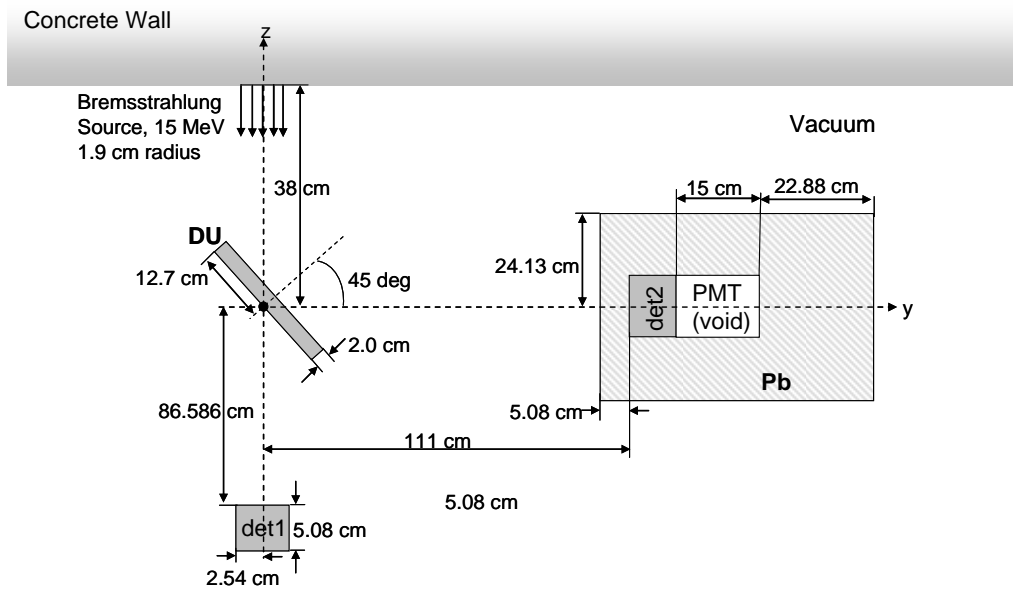


Fig. 2. Schematic of the MCNP-PoliMi model of the existing Idaho Accelerator Center experimental setup (not to scale).

Photon pulses from the collimator interact with the target, producing secondary particles; additionally, photons that do not interact serve as the trigger for the start detector. After the start signal, the stop detector is active to detect the secondary particles that arrive with some time distribution after the start detector is triggered (time = 0.0). The resulting distribution represents the time of flight of secondary particles arriving at the stop detector from the target and is shown in Fig. 3.

Data were taken for two different stop-detector distances (1.11 and 2.01 m). These resulting distributions are characterized by two bulk features: a sharp initial peak followed by a varying distribution. The initial peak signifies the arrival of the prompt gamma rays at the stop detector; all of the photons arrive at essentially the same time because they all travel at the same speed and start from approximately the same point. The subsequent distribution is the arrival of the generated neutrons at the stop detector. These secondary neutrons originate from three reactions: (γ, n) , $(\gamma, 2n)$, and $(\gamma, \text{fission})$. Each of these reactions has its own distinct energy distribution. The number of times each reaction occurs as well as the average energy of the neutrons released can be obtained from MCNPX ; this information is summarized in Table 1.

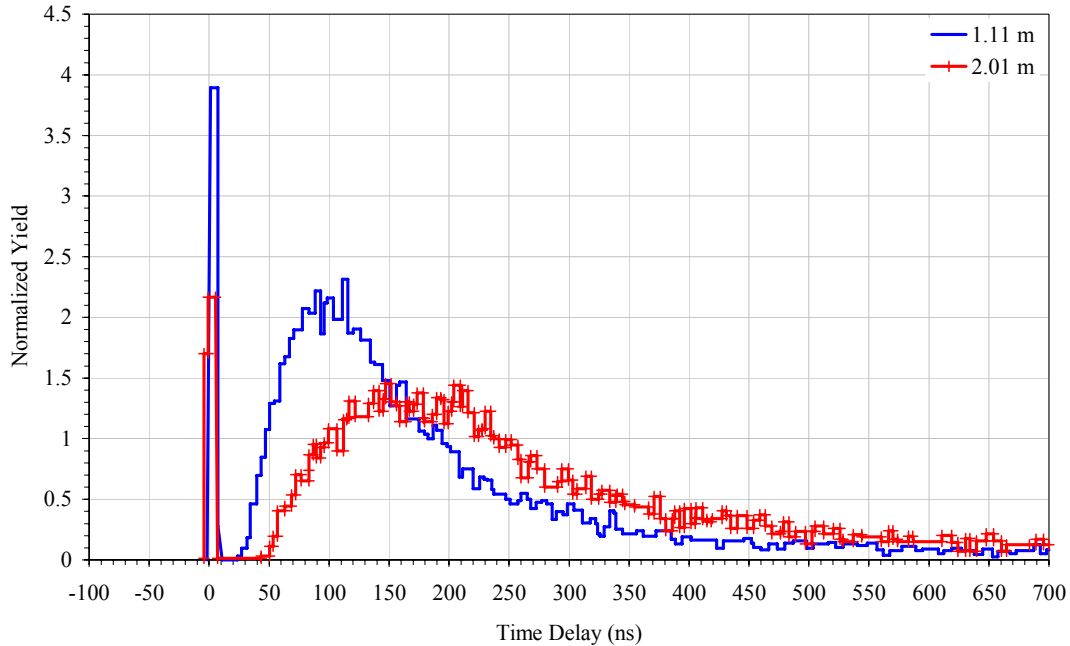


Fig. 3. Idaho Accelerator Center measurement results for bremsstrahlung interrogation of a depleted uranium target. Data are shown for two different stop-detector distances.

Table 1. Percentage and average energy of the three possible photonuclear reactions occurring in uranium-238 as obtained from MCNPX

Reaction	Percent of Total Reactions	Average Energy
(γ, n)	64.27%	918 keV
$(\gamma, 2n)$	24.15%	665 keV
$(\gamma, \text{fission})$	11.58%	2.0 MeV

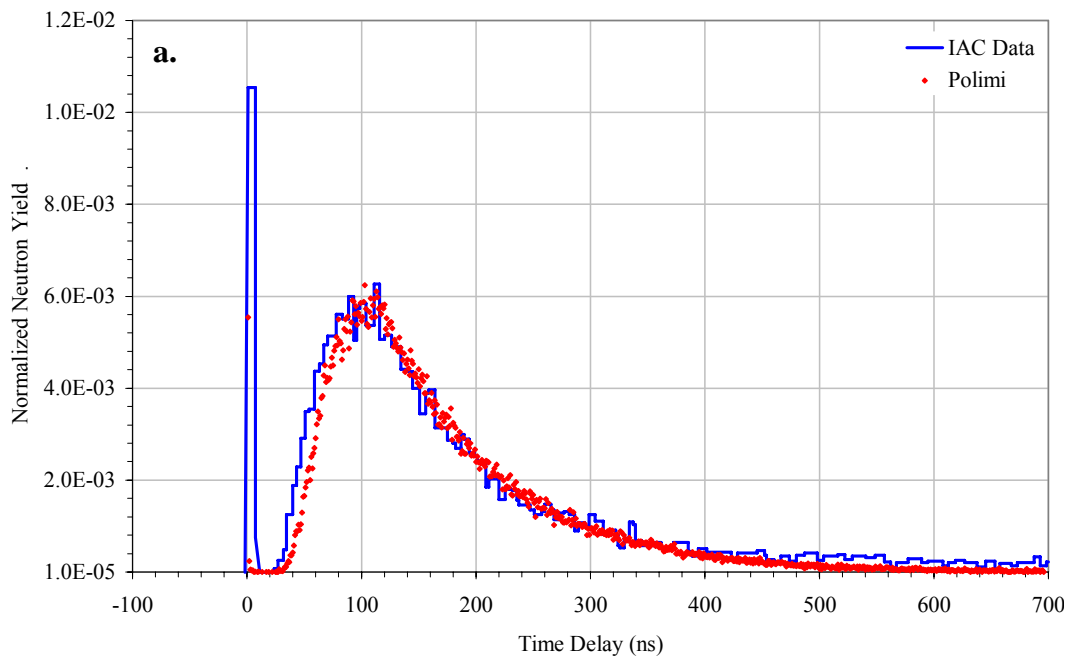
Each reaction produces a different number of neutrons, each of which has a different energy; these energy distributions directly correspond to a distribution of velocities. Assuming that each neutron originates from the same point, they will arrive at the detector at a time equal to the velocity times the fixed detector separation. Therefore, the peak time in the distribution corresponds to the detector separation times the average neutron velocity (energy). The data shown in Fig. 3 illustrate this result; the distribution at larger detector separation is shifted to later times as a result of the increased distance.

3. COMPARISON OF RESULTS

The simulations were performed by ORNL using the most current version of the MCNPX/MCNP-PoliMi code system. The full statistics of the neutron/photon field generated from photonuclear events were explicitly modeled. In addition, a detector-specific post-processing code was used to simulate the detector response to the incident particles; plastic scintillation detectors were simulated with a detection threshold of 0.006 MeVee. The system geometry shown in Fig. 2 was modeled, including a few assumptions that differed from the exact reality of the experimental setup. First, the linear

accelerator (LINAC) tungsten converter was omitted in the simulations. This approach is equivalent to assuming perfect collimation, which is valid considering the thickness of the concrete wall. Second, in the post-processing, some detector-specific properties such as threshold, dead time and pulse-generation time had to be assumed because they were not provided to ORNL by IAC. Finally, the data from IAC as well as the ORNL simulation results were normalized to the total number of neutron counts to allow a direct comparison. The results for both stop-detector separation distances are shown in Fig. 4.

For the 1.11-m separation case, the MCNP-PoliMi results agree very well over the full range of experimental data. There is some disagreement in the photon peak, which is attributable to the MCNP-PoliMi simulating only the particles from the photonuclear reactions. In reality some photons from the primary beam would be scattered into the stop detector. There is also a small discrepancy in the leading edge on the neutron distribution, which could have resulted from many possible sources. The neutrons that arrive at the detector in this short time have a very high velocity; thus, any small error in the geometric specifications of the experimental setup would have an exaggerated effect on the results. Also, the MCNP-PoliMi energy sampling of particles from these photonuclear reactions contains some approximations and assumptions. These assumptions could have propagated through the simulations and into the results. There is also some error at later times when the response is low. The extra detections not predicted by PoliMi could have come from background in the room or other scattering sources not included in the model.



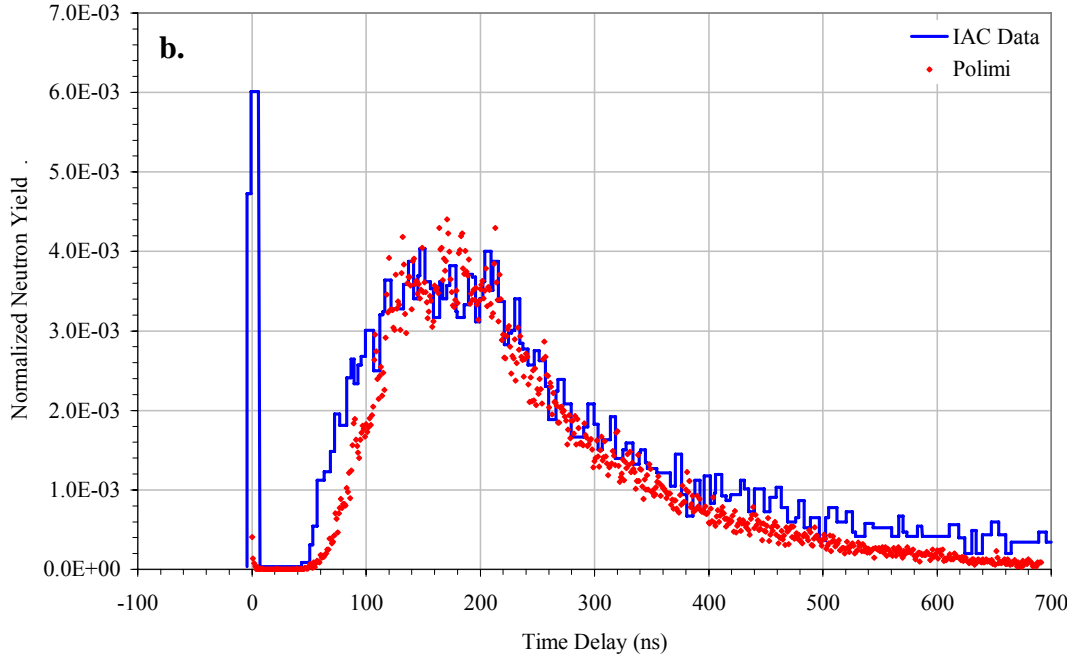


Fig. 4. Comparison of MCNP-PoliMi calculations to experimental data taken by Idaho Accelerator Center for (a) 1.11-m and (b) 2.01-m stop-detector separations.

From the MCNP-PoliMi output it is also possible to subdivide the total response into the specific neutron and gamma-ray contributions. These results are shown in Fig. 5 and serve to verify the proposed origin of the bulk features of the distribution. A small number of photons arrive at the stop detector at a time later than the primary peak. The origin of these photons could be absorption reactions in other system materials such as the concrete wall or the lead stop-detector shield.

In addition to individual particle contributions, it is also possible to group the signal by the originating photonuclear reaction. The results in Fig. 6 show that neutrons from fission have the smallest contribution to the total response, while neutrons from (γ, n) and $(\gamma, 2n)$ reactions have a nearly equal contribution. These results agree with the reaction percentage from MCNPX shown in Table 1, taking into account the fact that each $(\gamma, 2n)$ reaction produces two neutrons. Also, the peaks appear at approximately the same time for each reaction despite their differing average energies. The neutron velocity is proportional to the square root of the energy, and the time is proportional to the velocity. Therefore, the time is proportional to the square root of the energy, and the small difference in the average energy has a lessened effect on the resulting distribution.

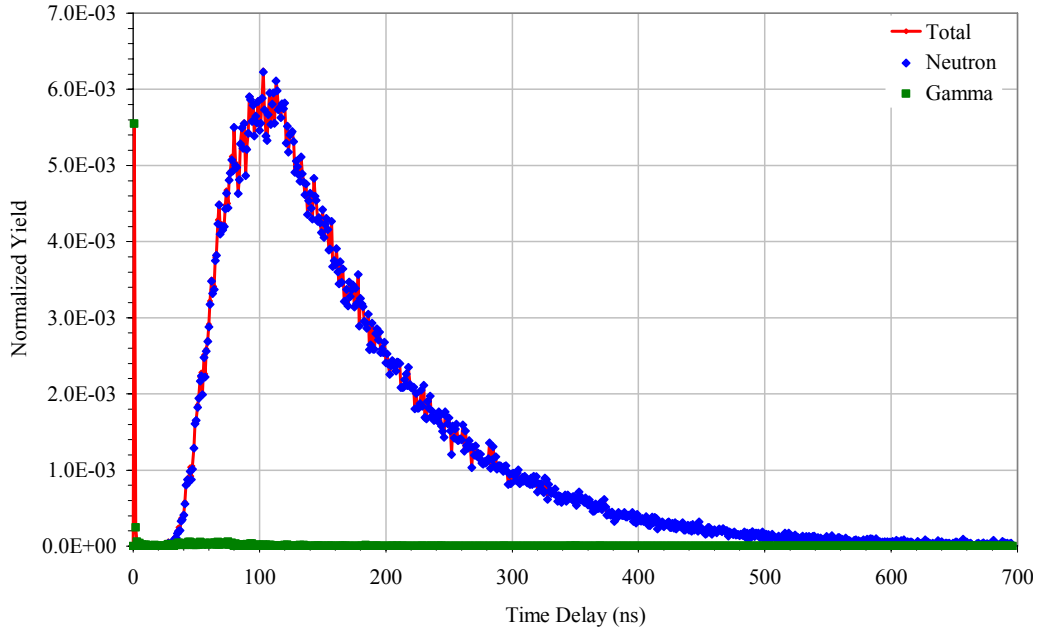


Fig. 5. MCNP-PoliMi simulation results for the existing experimental setup at 1.11-m stop-detector separation. Individual neutron and gamma-ray contributions to the total response are shown.

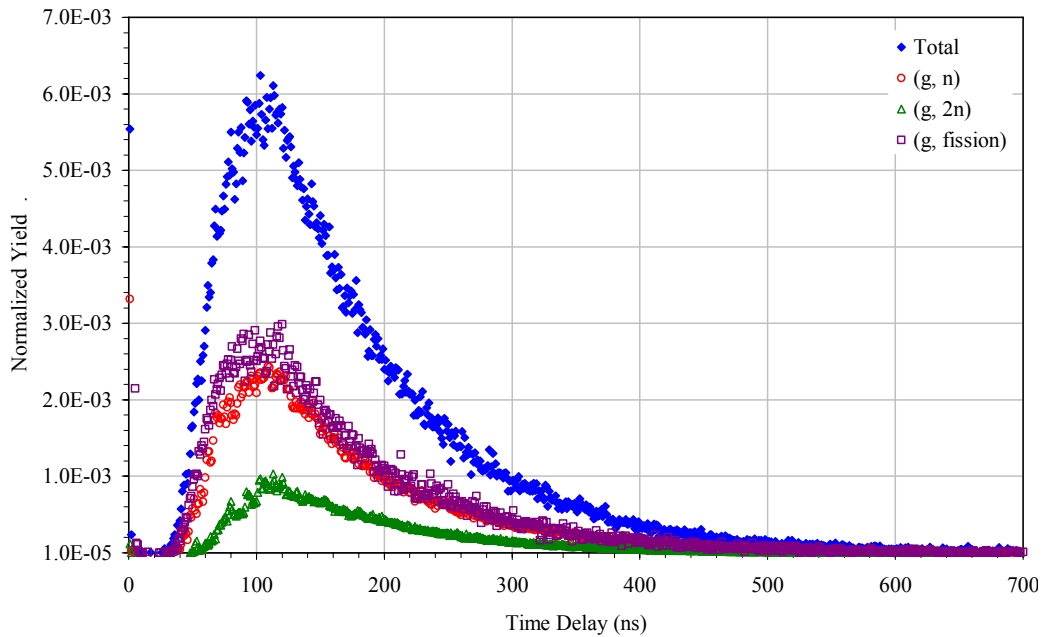


Fig. 6. MCNP-PoliMi simulation results for the existing experimental setup at 1.11-m stop-detector separation. Contributions to the total response from each photonuclear reaction are shown.

4. PROPOSED IAC EXPERIMENTAL SETUP

Previous results have shown MCNP-PoliMi to be capable of accurately modeling and reproducing the photon-interrogation measurements made at IAC. With this in mind, the

proposed experiment will be an extension of these prior time-of-flight measurements. Specifically, the proposed experiment will incorporate an additional stop detector to allow a correlation measurement. The proposed setup is shown in Fig. 7.

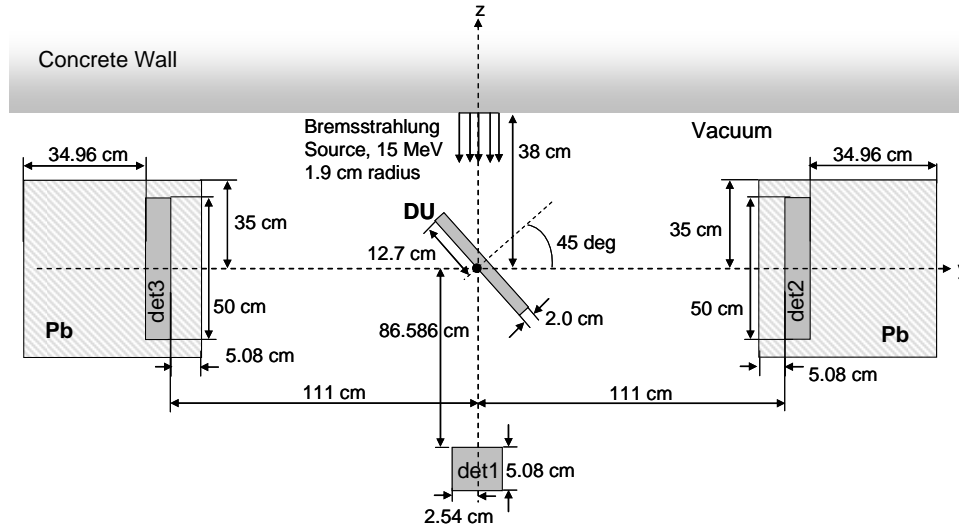


Fig. 7. Schematic of the MCNP-PoliMi model of the proposed Idaho Accelerator Center experimental setup (not to scale).

5. ANALYSIS OF PROPOSED SETUP

The proposed setup was analyzed using the MCNPX/MCNP-PoliMi code system; cross-correlation functions were generated for the same depleted uranium target and detectors as used in the existing setup. A lead target of the same dimensions was also simulated. Presented first, in Fig. 8, are the cross-correlation results for the depleted uranium target. The contributions from individual neutron and photon correlations are also shown. It is clear that the total detector signal consists largely of neutron–neutron correlations; in general, there are more prominent contributions from neutron–photon and photon–neutron events (typically on the order of the neutron–neutron events). In the experimental setup used here, there is a thick lead shield around each of the stop detectors, which shields the majority of the fission gamma rays. This setup explains the order-of-magnitude decrease in the number of neutron–photon events.

The use of the second stop detector in the system presents the possibility of detecting cross-talk events. A cross-talk event is recorded when a particle interacts in one stop detector, scatters into the second stop detector, and is recorded again; these events represent properties of only the system geometry, not of the fissions in the target material. Thus, it is desirable to minimize them in an attempt to measure the actual correlation events from the target material. The detector spacing in this system, as well as the lead shielding around the detectors, serves to reduce the number of cross-talk counts. Fig. 9 shows the distribution of these events within the total correlation function. The detector response has been subdivided into cross-talk events and other events; it is clear that the contribution of cross-talk events to the overall correlation function is negligible.

Therefore, the actual correlations can be distinguished from these cross-talk correlations during the proposed measurement.

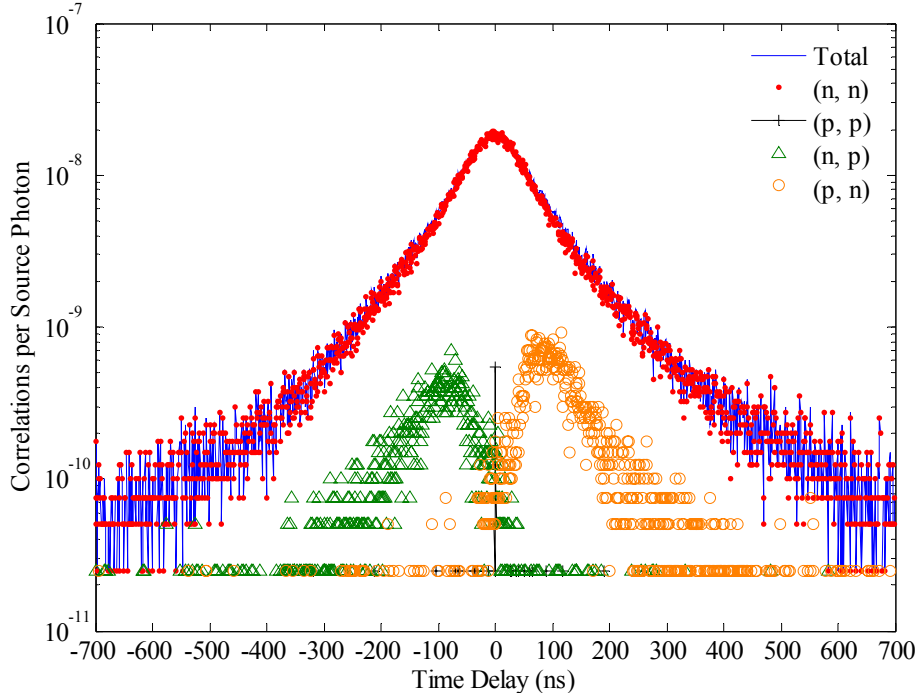


Fig. 8. MCNP-PoliMi-simulated cross-correlation function for proposed experimental configuration with a depleted uranium target. Separate neutron (n) and photon (p) contributions are shown.

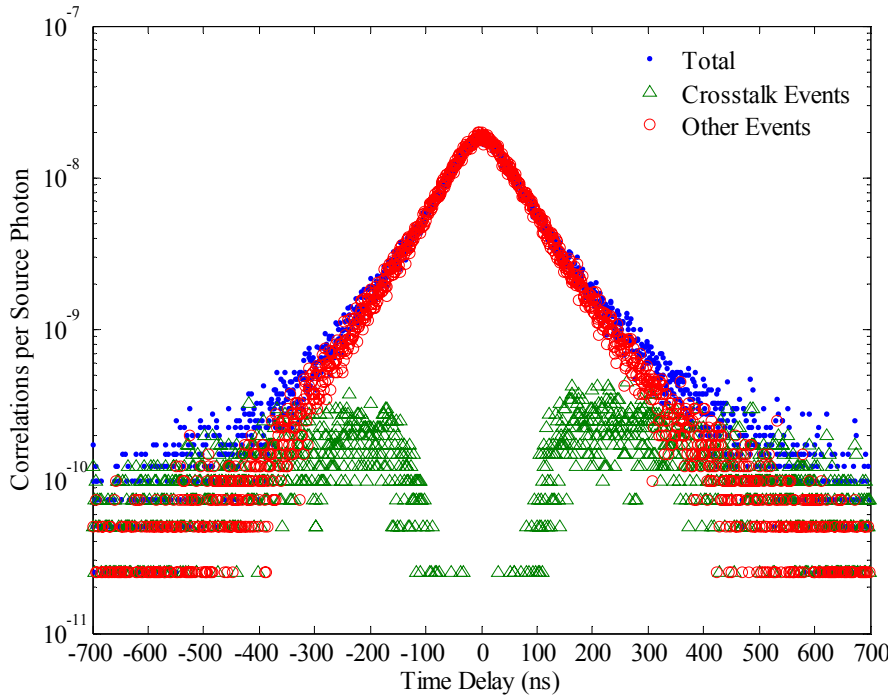


Fig. 9. MCNP-PoliMi-simulated cross-correlation function for proposed experimental configuration with a depleted uranium target. Contributions from cross-talk events are shown.

In addition to measuring the depleted uranium target, interrogation of a benign material is also planned for comparison. Because of its common use in radiation-shielding applications and ease of availability, lead will be used. The photonuclear cross section of lead is similar to that of depleted uranium (with a fission threshold at around 20 MeV); the photonuclear cross section consists of only the (γ, n) reaction, as shown in Fig. 10 (IAEA 2006). The composition of natural lead is 52.4% ^{208}Pb , 22.1% ^{207}Pb , 24.1% ^{206}Pb , and 1.4% ^{204}Pb . The photon energy corresponding to the cross-section peak in lead is approximately the same as in ^{238}U ; therefore, during photon interrogation one sees neutron emissions similar to those from a fissile target. However, the neutron multiplicity and energy distribution, as well as the multiplicity and energy of associated gamma rays, are quite different, which results in a dramatically different correlation function. The correlation function for a lead target is shown in Fig. 11.

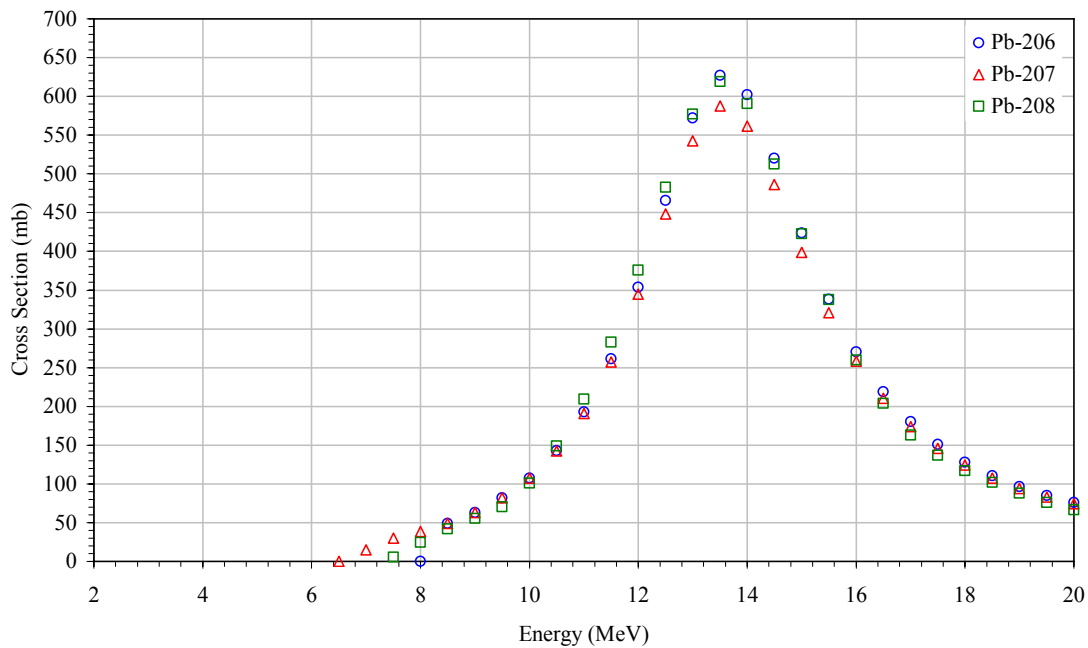


Fig. 10. Photonuclear cross sections for three common lead isotopes.

The correlation function with a lead target is similar to that using a uranium target (shown in Fig. 8) at later times; however, they appear to differ greatly at time delays close to zero. Also, there are many fewer neutron–neutron events than observed with the uranium target. This fact can be explained through the cross sections; uranium can undergo $(\gamma, 2n)$ and $(\gamma, \text{fission})$ in addition to (γ, n) . These additional reactions produce multiple neutrons, thereby increasing the probability of a correlated count at small time delays.

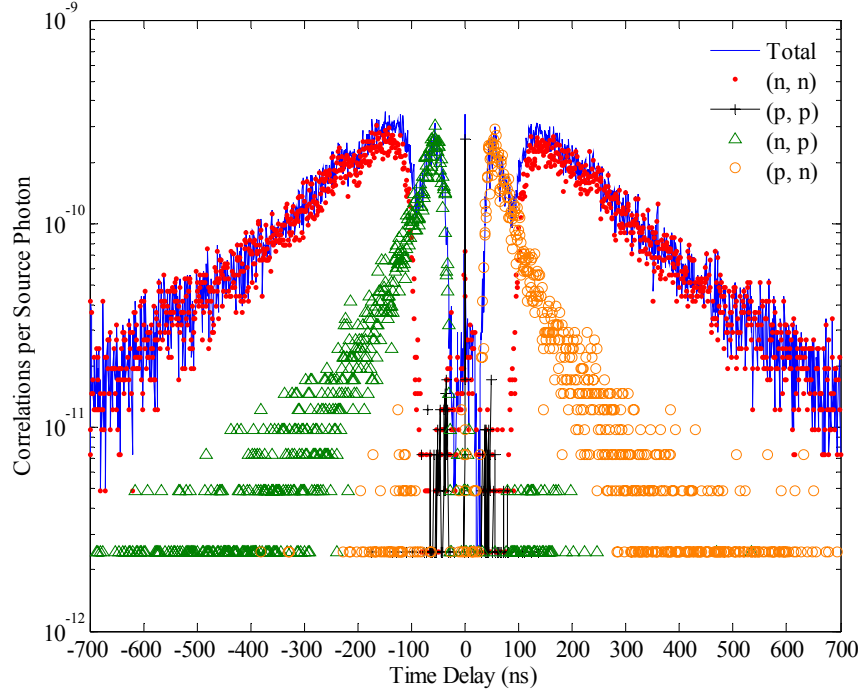


Fig. 11. MCNP-PoliMi-simulated cross-correlation function for proposed experimental configuration with a lead target. Separate neutron (n) and photon (p) contributions are shown.

The cross-talk contributions were also calculated for the lead target and are shown in Fig. 12. At first it might appear that many more cross-talk events occurred with the lead target, which would be unexpected because the geometry is exactly the same. In fact, there are simply many fewer true correlations with the lead target, making the cross-talk events dominant. A comparison of Fig. 6 and Fig. 12 makes it clear that the actual number of cross-talk events remains essentially constant (about 2×10^{-10} events at ± 200 ns), which follows from the previous argument regarding the number of multineutron reactions occurring in each target material.

The relative magnitude of the lead and uranium signals can be seen in Fig. 13. In the central region of the correlation function (from -250 to 250 ns), the uranium signal is approximately two orders of magnitude greater than that of lead. The outer regions of the signal are relatively close; however, this region of the signal consists largely of cross-talk events. Therefore, the correlation function of fissile material can be readily distinguished from a benign material, such as lead, when photonuclear events occur one at a time (i.e., not taking into account accidental coincidences caused by many photons arriving on the target simultaneously during actual LINAC operation).

As previously discussed in this report, the detection threshold was not specified for the detectors in question and was, thus, taken as a free variable for the data comparison in Chap. 3. This value was set as equal to 0.006 MeVee, which corresponds to approximately 47 keV of deposited neutron energy. This value is probably artificially lower than the detectors that will be used in the planned experiments. Therefore, additional correlations were generated using a larger, more realistic detection threshold of

500 keV of deposited neutron energy. A comparison of the lead and uranium correlation functions with this threshold is shown in Fig. 14.

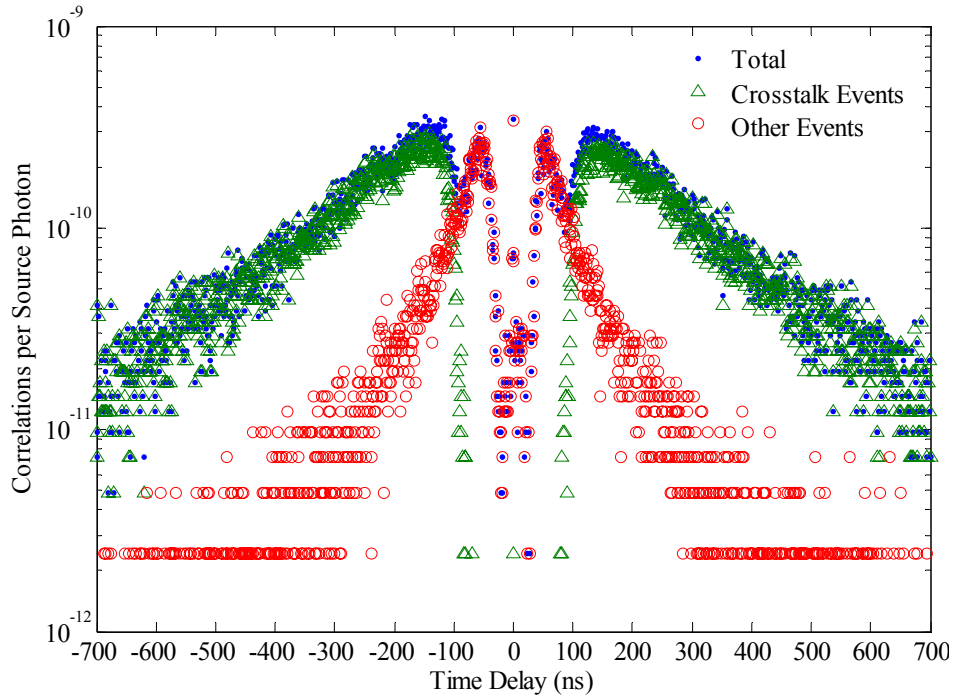


Fig. 12. MCNP-PoliMi-simulated cross-correlation function for proposed experimental configuration with a lead target. Contributions from cross-talk events are shown.

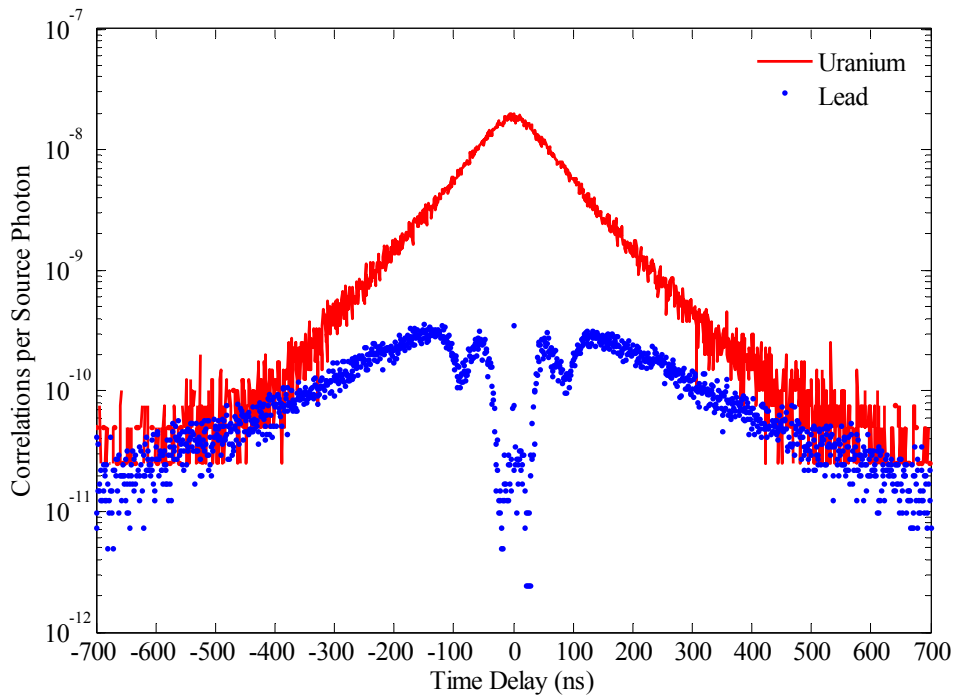


Fig. 13. Comparison of MCNP-PoliMi-simulated cross-correlation functions for depleted uranium and lead targets with a 47-keV detector threshold.

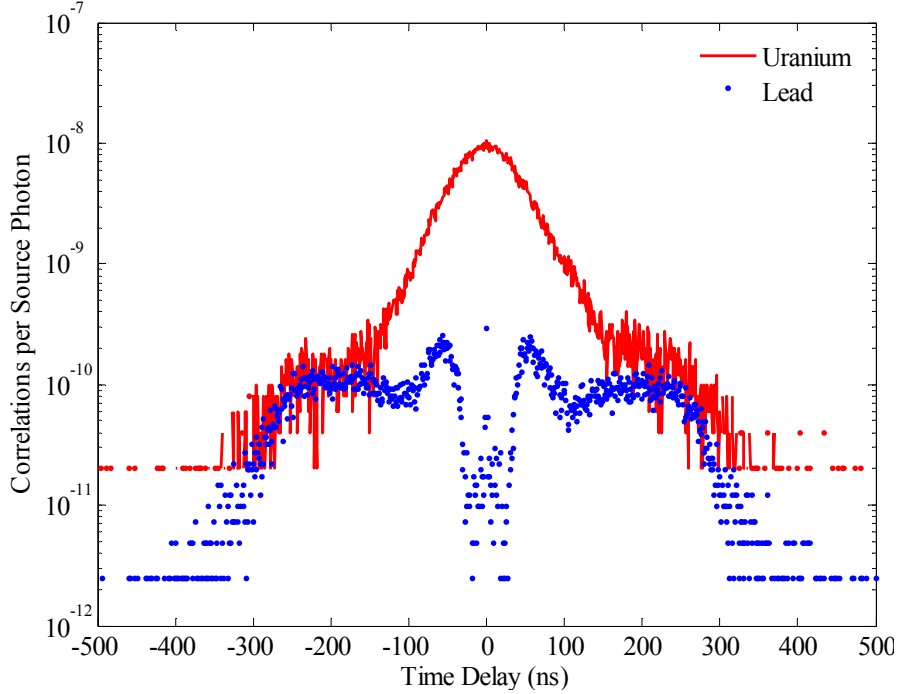


Fig. 14. Comparison of MCNP-PoliMi-simulated cross-correlation functions for depleted uranium and lead targets with a 500-keV detector threshold.

The bulk trends in the correlation functions remain unchanged, but there are fewer coincidences at later times. This trend corresponds to a reduction in the number of cross-talk events resulting from low-energy particles that have undergone some scattering interactions. The two signals are still readily distinguishable, and the reduction in cross-talk events could be advantageous while taking the actual data.

6. ANALYSIS OF ACCIDENTAL COINCIDENCES

Photons generated from a LINAC and used to interrogate nuclear and benign materials will arrive at the target in “bursts,” which is different from the behavior being modeled with the Monte Carlo method. The number of photons in a burst will depend on the electron current and the time structure of the LINAC. Details of the specific parameters of the LINAC operated at IAC are given in Table 2. The photon bursts generate a number of simultaneous photonuclear events in the target material. The number of photonuclear events for depleted uranium, highly enriched uranium, and lead are given in Table 3.

Table 2. Operational parameters of Idaho Accelerator Center LINAC

Beam current per pulse	0.3 nC
Pulse width	2 ns
Repetition rate	120 Hz
Counting time	1200–2400 s

Table 3. Number of photonuclear events occurring per source photon in various target materials.
Secondary neutron-induced fissions are shown for uranium targets.

Reaction	Depleted Uranium	Highly Enriched Uranium	Lead
(γ , n)	2.12×10^{-3}	1.55×10^{-3}	2.04×10^{-3}
(γ , 2n)	3.37×10^{-4}	7.62×10^{-5}	—
(γ , fission)	8.13×10^{-4}	1.51×10^{-3}	—
(n, fission)	7.66×10^{-5}	1.46×10^{-3}	—

The occurrence of many photonuclear events simultaneously generates coincident photons and neutrons, which in turn causes accidental coincidences in the detectors. These must be evaluated to obtain realistic estimates of measurement results. The evaluation of accidental coincidences can be performed on the basis of the target-detector time-of-flight signatures. The target-detector time of flight gives the neutron and gamma-ray probability of detection in each detector as a function of the time lag (i) between the photonuclear event at the target and the detection event at the detector.

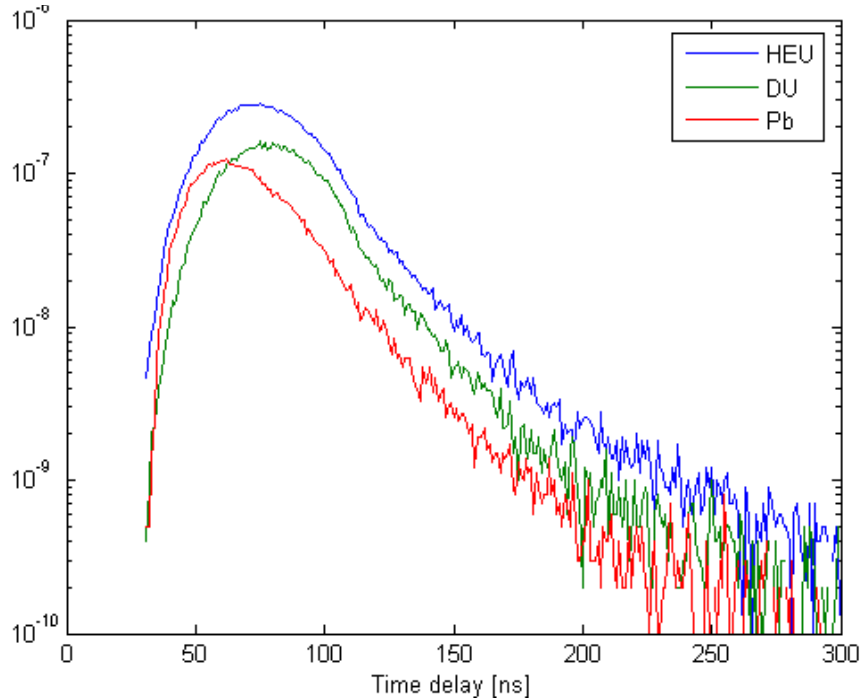


Fig. 15. Time of flight for three target materials: highly enriched uranium, depleted uranium, and lead.

The probability of detection at time delay i in one of the detectors is always much smaller than 1, which means that there are two possibilities: either one count is obtained with probability equal to the average number of counts, p_i , or no count is obtained, with probability $1-p_i$. Because either 0 or 1 count is sampled at the detectors, the probability of accidental pairs can be defined as the product of the two probabilities depending quadratic on source strength as follows:

$$APP(k) = \sum_i p_i \cdot p_{i+k} \cdot \quad (1)$$

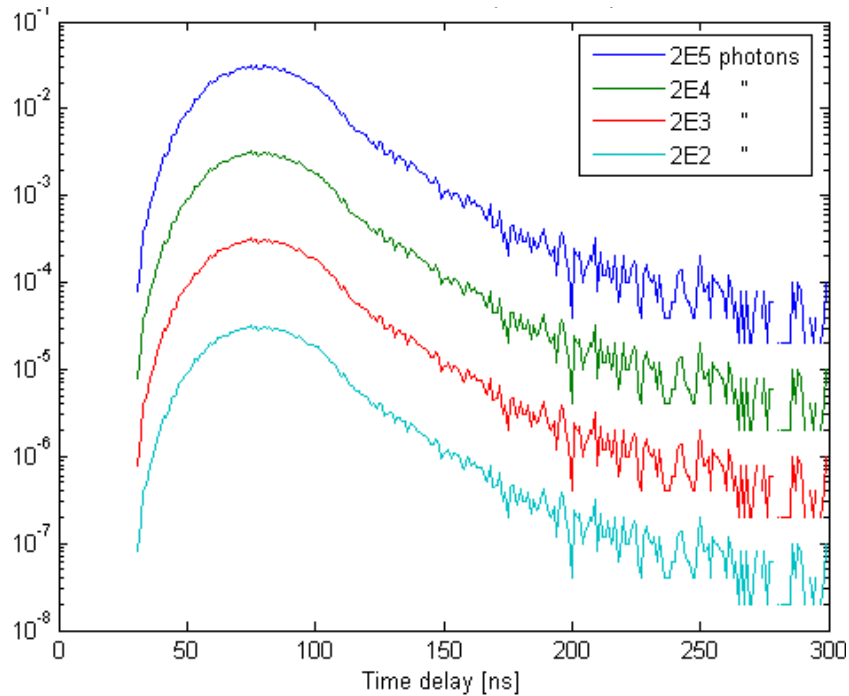


Fig. 16. Time-of-flight distributions for varying numbers of photons per burst for the depleted uranium target.

Fig. 17 shows the accidental coincidences originating from various groupings of $1e11$ photons—from $5e5$ pulses each of $2e5$ photons to $5e8$ pulses each of $2e2$ photons. The figure shows that this latter case is the only one in which the accidental coincidences are fewer than the real coincidences. This measurement would take 83 min using an accelerator operating at 100 kHz.

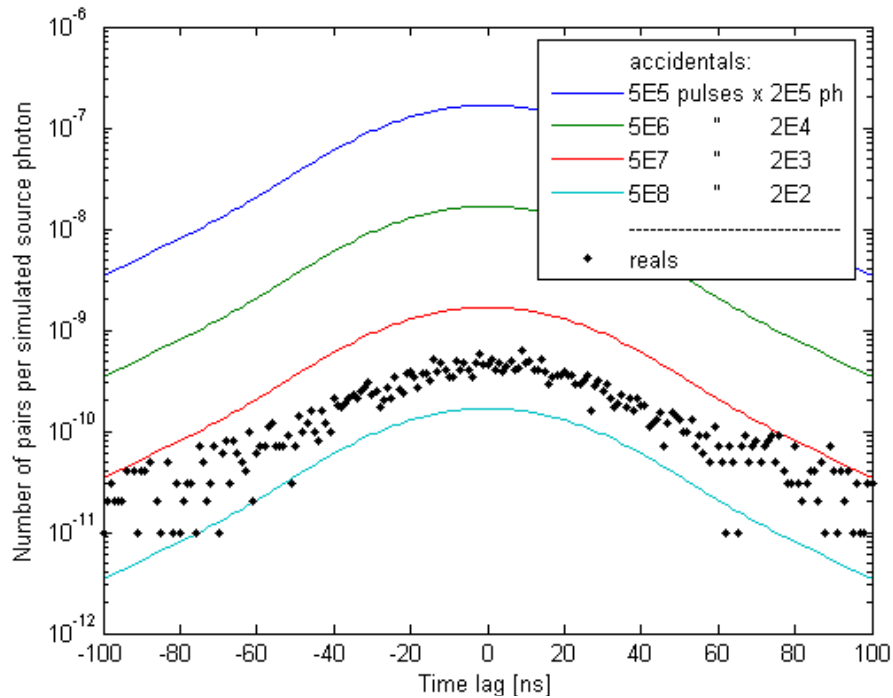


Fig. 17. Distribution of real and accidental coincidences for the depleted uranium target.

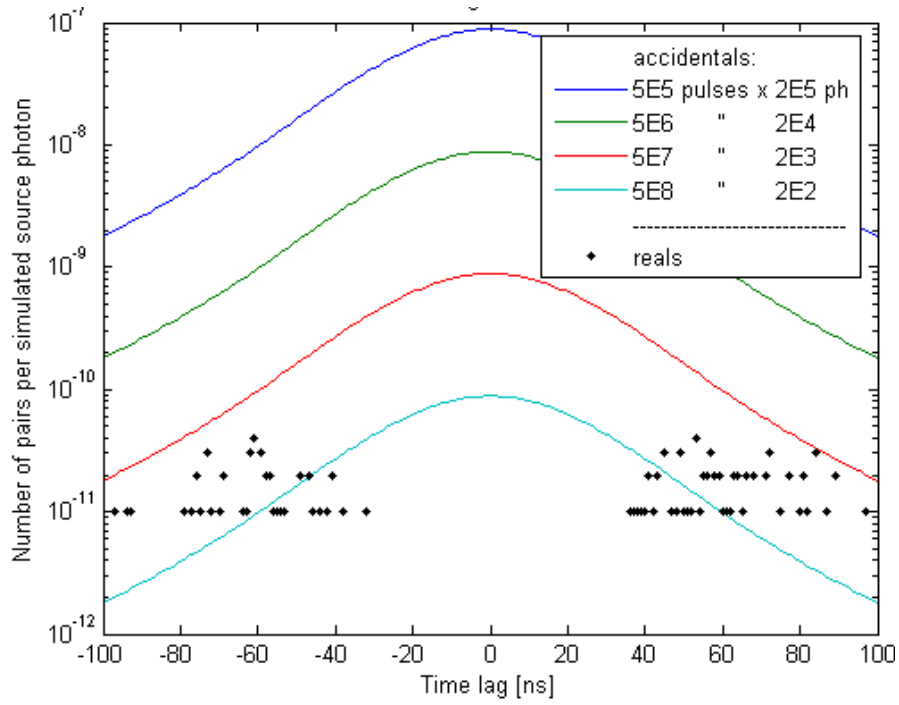


Fig. 18. Distribution of real and accidental coincidences for the lead target.

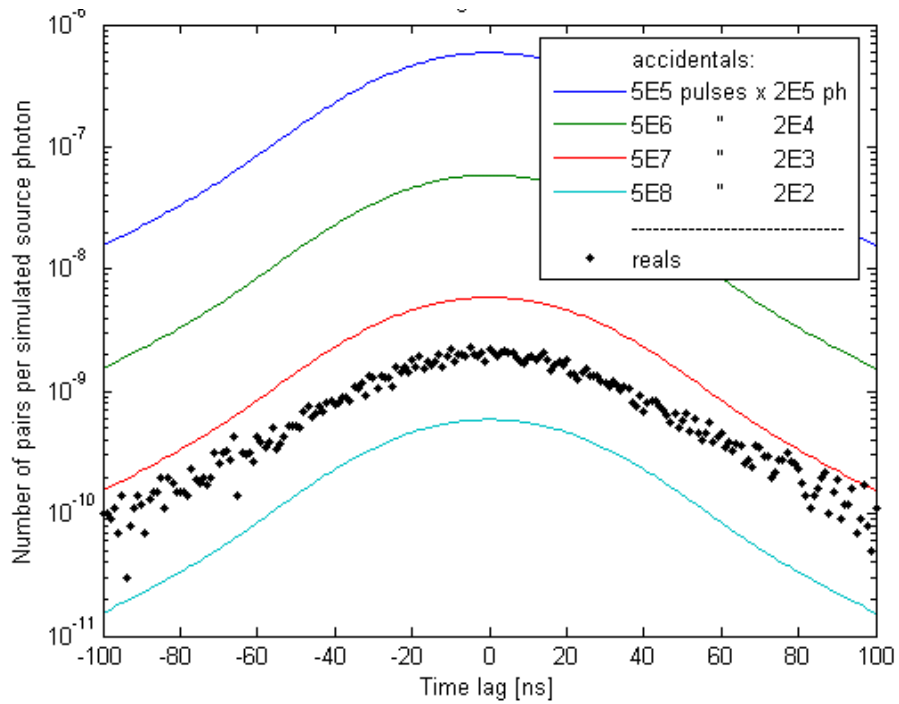


Fig. 19. Distribution of real and accidental coincidences for the highly enriched uranium target.

7. DISCUSSION AND CONCLUSIONS

Based on the comparison of results in Chap. 3, it is clear that the MCNPX/MCNP-PoliMi code system is capable of accurately predicting the correlated-detector response to uranium interrogation with high-energy photons. In fact, this code system calculates the full statistics of the neutron/photon field directly resulting from photonuclear interactions. This information is then sent to a detector-specific post-processor; plastic scintillation detectors were simulated in this work. The detector physics are simulated, and the time correlations are determined. The result is a code system that simulates the full interrogation process, from source to detector response, resulting in a very accurate calculation.

The proven accuracy of these results enabled ORNL to use the MCNPX/MCNP-PoliMi code system to plan future experiments. Specifically, measurements have been planned that implement two stop detectors to perform correlation measurements on a photon-interrogated uranium target. Calculations have shown the number of false coincidences coming from cross-talk events to be negligible for a uranium target. However, there will be considerable background in the target room, which has not yet been simulated and must be overcome during the measurement. In addition, there will be a considerable flash of prompt fission gamma rays as well as scattered source photons that could overwhelm the detector; the lead shielding around the stop detectors or appropriate gating of the detector photomultiplier tubes will help solve this problem.

Calculations have also been performed replacing the uranium target with a natural lead one. Lead does have a photonuclear neutron production cross section by means of a (γ, n) reaction that peaks at approximately the same incident photon energy as the uranium cross sections. These reactions also have associated gamma rays and therefore can produce a detector response similar to that observed in the interrogation of fissile material. However, it has been shown that the lack of multineutron-producing reactions in lead leads to a dramatically different correlated-detector response. The response of benign nuclear materials to interrogation is of interest to applications in homeland security.

A study of the occurrence of accidental coincidences resulting from photon bursts that interact with the target material has shown that the proposed correlation measurements are feasible only with an accelerator time structure of the order of 100 kHz emitting up to a few hundred photons per burst. Future work will include the study of multiplicities measured using multiple detectors.

8. ACKNOWLEDGMENT

ORNL is managed and operated for the Department of Energy by UT-Battelle, LLC, under contract DE-AC05-00OR22725. This work was supported in part by the Department of Energy National Nuclear Security Administration NA-241.

9. REFERENCES

- IAEA Photonuclear Data 2006. "Photonuclear Evaluations and Plots." <http://t2.lanl.gov/data/photonuclear.html>, May 31, 2006.
- Pozzi, S. A., E. Padovani, and M. Marseguerra. 2003. "MCNP-PoliMi: A Monte Carlo Code for Correlation Measurements." *Nuclear Instruments and Methods* **A513**: 550–558.

APPENDIX A
MCNPX INPUT FILE

MCNPX Input File

```
IAC brem interrogation of a uranium target
c CELL CARDS
c
c uranium target
100 1 -19.1 -101 imp:n,p=1
c
c detector one
c 200 2 -1.032 -201 imp:p,n=1
200 0 -201 imp:p,n=1
c
c detector two
c 300 2 -1.032 -301 imp:p,n=1
300 0 -301 imp:p,n=1
c
c detector three
c 400 2 -1.032 -401 imp:p,n=1
400 0 -401 imp:p,n=1
c
c detector two shield
c 500 3 -11.34 -501 301 imp:p,n=1
500 0 -501 301 imp:p,n=1
c
c detector three shield
c 600 3 -11.34 -601 401 imp:p,n=1
600 0 -601 401 imp:p,n=1
c
c concrete wall
c 700 4 -2.2505 -701 imp:p,n=1
700 0 -701 imp:p,n=1
c
c bounding volume
800 0 -801 501 601 #100 #200 #700 imp:p,n=1
c
c outside world
900 0 801 imp:p,n=0
c END CELL CARDS-BLANK LINE FOLLOWS

c SURFACE CARDS
c
c uranium target
101 rcc 0 0 0 0 1.4142 1.4142 12.7
c
c detector one
201 rcc 0 0 -86.586 0 0 -5.08 2.54
c
c detector two
301 box -12.5 111 -12.5 25 0 0 0 8 0 0 0 25
c
c detector three
401 box -12.5 -119 -12.5 25 0 0 0 8 0 0 0 25
c
c detector two shield
501 box -24.13 105.92 -24.13 48.26 0 0 0 48.04 0 0 0 48.26
c
c detector three shield
601 box -24.13 -153.96 -24.13 48.26 0 0 0 48.04 0 0 0 48.26
c
c concrete wall
701 box -50 -160 38 100 0 0 0 320 0 0 0 50
```

```

c
c bounding box
801 rpp -51 51 -161 161 -100 90
c
c source plane
999 pz 37.9999
c END SURFACE CARDS-BLANK LINE FOLLOWS

c DATA CARDS
c
c Brem photon source along z-axis with 1.9cm radius
sdef par=2 sur=999 pos=0.0 0.0 37.9999 dir=-1 rad=d1 erg=d2
sil 1.9
si2 3.0000 3.1000 3.2000 3.3000 3.4000
3.5000 3.6000 3.7000 3.8000 3.9000 4.0000 4.1000
4.2000 4.3000 4.4000 4.5000 4.6000 4.7000 4.8000
4.9000 5.0000 5.1000 5.2000 5.3000 5.4000 5.5000
5.6000 5.7000 5.8000 5.9000 6.0000 6.1000 6.2000
6.3000 6.4000 6.5000 6.6000 6.7000 6.8000 6.9000
7.0000 7.1000 7.2000 7.3000 7.4000 7.5000 7.6000
7.7000 7.8000 7.9000 8.0000 8.1000 8.2000 8.3000
8.4000 8.5000 8.6000 8.7000 8.8000 8.9000 9.0000
9.1000 9.2000 9.3000 9.4000 9.5000 9.6000 9.7000
9.8000 9.9000 10.0000 10.1000 10.2000 10.3000 10.4000
10.5000 10.6000 10.7000 10.8000 10.9000 11.0000 11.1000
11.2000 11.3000 11.4000 11.5000 11.6000 11.7000 11.8000
11.9000 12.0000 12.1000 12.2000 12.3000 12.4000 12.5000
12.6000 12.7000 12.8000 12.9000 13.0000 13.1000 13.2000
13.3000 13.4000 13.5000 13.6000 13.7000 13.8000 13.9000
14.0000 14.1000 14.2000 14.3000 14.4000 14.5000 14.6000
14.7000 14.8000 14.9000 15.0000
sp2 0.0000 0.0055 0.0052 0.0050 0.0048
0.0044 0.0044 0.0043 0.0040 0.0041 0.0037 0.0034
0.0035 0.0034 0.0031 0.0030 0.0029 0.0030 0.0027
0.0026 0.0026 0.0025 0.0025 0.0023 0.0023 0.0022
0.0023 0.0020 0.0020 0.0019 0.0018 0.0018 0.0019
0.0017 0.0017 0.0017 0.0017 0.0015 0.0015 0.0014
0.0015 0.0014 0.0013 0.0013 0.0013 0.0012 0.0012
0.0013 0.0012 0.0011 0.0011 0.0011 0.0011 0.0010
0.0011 0.0010 0.0010 0.0010 0.0009 0.0009 0.0009
0.0009 0.0009 0.0008 0.0009 0.0009 0.0008 0.0007
0.0007 0.0007 0.0007 0.0007 0.0007 0.0006 0.0006
0.0006 0.0006 0.0006 0.0006 0.0006 0.0006 0.0006
0.0005 0.0005 0.0005 0.0005 0.0005 0.0005 0.0004
0.0005 0.0004 0.0005 0.0004 0.0004 0.0004 0.0004
0.0003 0.0004 0.0004 0.0004 0.0003 0.0003 0.0003
0.0003 0.0003 0.0003 0.0002 0.0002 0.0002 0.0002
0.0002 0.0002 0.0001 0.0002 0.0001 0.0001 0.0001
0.0001 0.0001 0.0001 0.0000

c
c MATERIAL DEFINITIONS
c uranium target
m1 plib=02p nlib=60c
92238 1.00
c
c plastic detector
m2 plib=02p nlib=60c
1001 0.5246
6000 0.4754
mpn2 0 0
c
c detector shield
m3 plib=02p nlib=60c

```

```

      82206  -0.241
      82207  -0.221
      82208  -0.524
mpn3 0 0 0
c
c concrete
m4  plib=02p  nlib=60c
      1001   8.47636e-2
      8016   6.04086e-1
      11023  9.47250e-3
      12000  2.99826e-3
      13027  2.48344e-2
      14000  2.41860e-1
      19000  6.85513e-3
      20000  2.04808e-2
      26054  2.74322e-4
      26056  4.26455e-3
      26057  9.76401e-5
      26058  1.30187e-5
mpn4 0 0 0 0 0 0 0 0 0 0 0 0 0
c
MODE      N P
PHYS:P    0 2J  -1
CUT:P     J 0.19 0
DBCN      12J 2001
NPS       1E9
PRINT     10 40 50 110 126 140
TOTNU
IDUM      55
RDUM      3J 3.
FILES     10J 55 iacdat

```


APPENDIX B

MCNP-POLIMI INPUT FILE FOR EXISTING EXPERIMENTAL GEOMETRY

MCNP-PoliMi Input File for Existing Experimental Geometry

```
Brem interrogation of a uranium target - POLIMI
c CELL CARDS
c
c uranium target
100 1 -19.1 -101 imp:n,p=1
c
c detector one
200 2 -1.032 -201 imp:p,n=1
c
c detector two
300 2 -1.032 -301 imp:p,n=1
c
c detector two PMT region
400 0 -401 imp:p,n=1
c detector two shield
500 3 -11.34 -501 (401 301) imp:p,n=1
c bounding volume
600 0 -601 501 #100 #200 imp:p,n=1
c
c outside world
700 0 601 imp:p,n=0
c END CELL CARDS-BLANK LINE FOLLOWS

c SURFACE CARDS
c
c uranium target
101 rcc 0 0 0 0 1.4142 1.4142 12.7
c
c detector one
201 rcc 0 0 -86.586 0 0 -5.08 2.54
c
c detector two
301 rcc 0 111 0 0 5.08 0 2.54
c
c detector two PMT region
401 rcc 0 116.08 0 0 15 0 2.54
c
c detector two shield
501 rcc 0 105.92 0 0 48.04 0 24.13
c
c bounding box
601 rpp -25 25 -30 160 -100 50
c
c source plane
999 pz 38.0
c
c END SURFACE CARDS-BLANK LINE FOLLOWS

c DATA CARDS
c
c Brem photon source along z-axis with 1.9cm radius
sdef par=2 sur=999 pos=0.0 0.0 38.0 dir=-1 rad=d1 erg=d2
sil 1.9
si2 3.0000 3.1000 3.2000 3.3000 3.4000
3.5000 3.6000 3.7000 3.8000 3.9000 4.0000 4.1000
4.2000 4.3000 4.4000 4.5000 4.6000 4.7000 4.8000
4.9000 5.0000 5.1000 5.2000 5.3000 5.4000 5.5000
5.6000 5.7000 5.8000 5.9000 6.0000 6.1000 6.2000
6.3000 6.4000 6.5000 6.6000 6.7000 6.8000 6.9000
```

	7.0000	7.1000	7.2000	7.3000	7.4000	7.5000	7.6000
	7.7000	7.8000	7.9000	8.0000	8.1000	8.2000	8.3000
	8.4000	8.5000	8.6000	8.7000	8.8000	8.9000	9.0000
	9.1000	9.2000	9.3000	9.4000	9.5000	9.6000	9.7000
	9.8000	9.9000	10.0000	10.1000	10.2000	10.3000	10.4000
	10.5000	10.6000	10.7000	10.8000	10.9000	11.0000	11.1000
	11.2000	11.3000	11.4000	11.5000	11.6000	11.7000	11.8000
	11.9000	12.0000	12.1000	12.2000	12.3000	12.4000	12.5000
	12.6000	12.7000	12.8000	12.9000	13.0000	13.1000	13.2000
	13.3000	13.4000	13.5000	13.6000	13.7000	13.8000	13.9000
	14.0000	14.1000	14.2000	14.3000	14.4000	14.5000	14.6000
	14.7000	14.8000	14.9000	15.0000			
sp2	0.0000	0.0055	0.0052	0.0050	0.0048		
	0.0044	0.0044	0.0043	0.0040	0.0041	0.0037	0.0034
	0.0035	0.0034	0.0031	0.0030	0.0029	0.0030	0.0027
	0.0026	0.0026	0.0025	0.0025	0.0023	0.0023	0.0022
	0.0023	0.0020	0.0020	0.0019	0.0018	0.0018	0.0019
	0.0017	0.0017	0.0017	0.0017	0.0015	0.0015	0.0014
	0.0015	0.0014	0.0013	0.0013	0.0013	0.0012	0.0012
	0.0013	0.0012	0.0011	0.0011	0.0011	0.0011	0.0010
	0.0011	0.0010	0.0010	0.0010	0.0009	0.0009	0.0009
	0.0009	0.0009	0.0008	0.0009	0.0009	0.0008	0.0007
	0.0007	0.0007	0.0007	0.0007	0.0007	0.0006	0.0006
	0.0006	0.0006	0.0006	0.0006	0.0006	0.0006	0.0006
	0.0005	0.0005	0.0005	0.0005	0.0005	0.0005	0.0004
	0.0005	0.0004	0.0005	0.0004	0.0004	0.0004	0.0004
	0.0003	0.0004	0.0004	0.0004	0.0003	0.0003	0.0003
	0.0003	0.0003	0.0003	0.0002	0.0002	0.0002	0.0002
	0.0002	0.0002	0.0001	0.0002	0.0001	0.0001	0.0001
	0.0001	0.0001	0.0001	0.0000			

```

c
c MATERIAL DEFINITIONS
c uranium target
m1 plib=02p nlib=50c
   92238 1.00
c
c plastic detector
m2 plib=02p nlib=60c
   1001 0.5246
   6000 0.4754
c
c detector shield
m3 plib=02p nlib=50c
   82000 1.00
c
c air
c m4 plib=02p nlib=50c
c   7014 0.6869
c   8016 0.3012
c   6012 0.0001
c   18040 0.0117
c mpn 0 0 0 0
c
c MISC PARAMETERS
c
MODE N P
PHYS:N J 20
PHYS:P 0 1 1
CUT:P 2J 0
NPS 1
PRINT 10 40 50 110 126 140
DBCN 12J 6001
TOTNU

```

```
IDUM 55 1 2 1 125 1 2 200 300  
RDUM 0.001 0.001 J J J 1000 9E4  
FILES 21 brem.d J U 6J 55 bremdat1
```


APPENDIX C

**MCNP-POLIMI INPUT FILE FOR PROPOSED EXPERIMENTAL
GEOMETRY**

MCNP-PoliMi Input File for Proposed Experimental Geometry

```
IAC brem interrogation of a uranium target using 2 stop detectors - POLIMI
c CELL CARDS
c
c uranium target
100 1 -19.1 -101 imp:n,p=1
c
c detector one
200 2 -1.032 -201 imp:p,n=1
c
c detector two
300 2 -1.032 -301 imp:p,n=1
c
c detector three
400 2 -1.032 -401 imp:p,n=1
c
c detector two shield
500 3 -11.34 -501 301 imp:p,n=1
c
c detector three shield
600 3 -11.34 -601 401 imp:p,n=1
c
c concrete wall
700 4 -2.2505 -701 imp:p,n=1
c
c bounding volume
800 0 -801 501 601 #100 #200 #700 imp:p,n=1
c
c outside world
900 0 801 imp:p,n=0
c END CELL CARDS-BLANK LINE FOLLOWS

c SURFACE CARDS
c
c uranium target
101 rcc 0 0 0 0 1.4142 1.4142 12.7
c
c detector one
201 rcc 0 0 -86.586 0 0 -5.08 2.54
c
c detector two
301 box -25 111 -25 50 0 0 0 8 0 0 0 50
c
c detector three
401 box -25 -111 -25 50 0 0 0 -8 0 0 0 50
c
c detector two shield
501 box -35 105.92 -35 70 0 0 0 48.04 0 0 0 70
c
c detector three shield
601 box -35 -105.92 -35 70 0 0 0 -48.04 0 0 0 70
c
c concrete wall
701 box -50 -160 38 100 0 0 0 320 0 0 0 50
c
c bounding box
801 rpp -51 51 -161 161 -100 90
c
c source plane
999 pz 37.9999
```

c END SURFACE CARDS-BLANK LINE FOLLOWS

c DATA CARDS

c

c Brem photon source along z-axis with 1.9cm radius

sdef par=2 sur=999 pos=0.0 0.0 37.9999 dir=-1 rad=d1 erg=d2

sil 1.9

si2	3.0000	3.1000	3.2000	3.3000	3.4000		
	3.5000	3.6000	3.7000	3.8000	3.9000	4.0000	4.1000
	4.2000	4.3000	4.4000	4.5000	4.6000	4.7000	4.8000
	4.9000	5.0000	5.1000	5.2000	5.3000	5.4000	5.5000
	5.6000	5.7000	5.8000	5.9000	6.0000	6.1000	6.2000
	6.3000	6.4000	6.5000	6.6000	6.7000	6.8000	6.9000
	7.0000	7.1000	7.2000	7.3000	7.4000	7.5000	7.6000
	7.7000	7.8000	7.9000	8.0000	8.1000	8.2000	8.3000
	8.4000	8.5000	8.6000	8.7000	8.8000	8.9000	9.0000
	9.1000	9.2000	9.3000	9.4000	9.5000	9.6000	9.7000
	9.8000	9.9000	10.0000	10.1000	10.2000	10.3000	10.4000
	10.5000	10.6000	10.7000	10.8000	10.9000	11.0000	11.1000
	11.2000	11.3000	11.4000	11.5000	11.6000	11.7000	11.8000
	11.9000	12.0000	12.1000	12.2000	12.3000	12.4000	12.5000
	12.6000	12.7000	12.8000	12.9000	13.0000	13.1000	13.2000
	13.3000	13.4000	13.5000	13.6000	13.7000	13.8000	13.9000
	14.0000	14.1000	14.2000	14.3000	14.4000	14.5000	14.6000
	14.7000	14.8000	14.9000	15.0000			
sp2	0.0000	0.0055	0.0052	0.0050	0.0048		
	0.0044	0.0044	0.0043	0.0040	0.0041	0.0037	0.0034
	0.0035	0.0034	0.0031	0.0030	0.0029	0.0030	0.0027
	0.0026	0.0026	0.0025	0.0025	0.0023	0.0023	0.0022
	0.0023	0.0020	0.0020	0.0019	0.0018	0.0018	0.0019
	0.0017	0.0017	0.0017	0.0017	0.0015	0.0015	0.0014
	0.0015	0.0014	0.0013	0.0013	0.0013	0.0012	0.0012
	0.0013	0.0012	0.0011	0.0011	0.0011	0.0011	0.0010
	0.0011	0.0010	0.0010	0.0010	0.0009	0.0009	0.0009
	0.0009	0.0009	0.0008	0.0009	0.0009	0.0008	0.0007
	0.0007	0.0007	0.0007	0.0007	0.0007	0.0006	0.0006
	0.0006	0.0006	0.0006	0.0006	0.0006	0.0006	0.0006
	0.0005	0.0005	0.0005	0.0005	0.0005	0.0005	0.0004
	0.0005	0.0004	0.0005	0.0004	0.0004	0.0004	0.0004
	0.0003	0.0004	0.0004	0.0004	0.0003	0.0003	0.0003
	0.0003	0.0003	0.0003	0.0002	0.0002	0.0002	0.0002
	0.0002	0.0002	0.0001	0.0002	0.0001	0.0001	0.0001
	0.0001	0.0001	0.0001	0.0000			

c

c MATERIAL DEFINITIONS

c uranium target

m1 plib=02p nlib=60c
92238 1.00

c

c plastic detector

m2 plib=02p nlib=60c
1001 0.5246
6000 0.4754

c mpn2 0 0

c

c detector shield

m3 plib=02p nlib=60c
82206 -0.241
82207 -0.221
82208 -0.524

c mpn3 0 0 0

c

c concrete

```
m4 plib=02p nlib=60c
  1001  8.47636e-2
  8016  6.04086e-1
 11023  9.47250e-3
 12000  2.99826e-3
 13027  2.48344e-2
 14000  2.41860e-1
 19000  6.85513e-3
 20000  2.04808e-2
 26054  2.74322e-4
 26056  4.26455e-3
 26057  9.76401e-5
 26058  1.30187e-5
c mpn4 0 0 0 0 0 0 0 0 0 0 0 0
c
MODE N P
PHYS:N J 20
PHYS:P 0 1 1
CUT:P 2J 0
NPS 1
PRINT 10 40 50 110 126 140
DBCN 12J 20001
TOTNU
IDUM 55 1 2 1 40 2 3 200 300 400
RDUM 0.001 0.001 J J J 1000 9E4
FILES 21 iac3.d J U 6J 55 iacdat3
LOST 10000 10000
```


INTERNAL DISTRIBUTION

1. S.A. Pozzi
2. J.T. Mihalczo
3. P. Hausladen
4. J. Radle
5. M. Flaska

EXTERNAL DISTRIBUTION

6. E. Padovani, Polytechnic of Milan, Milan, Italy
7. T.J. Downar, Purdue University, 400 Central Drive, West Lafayette, IN 47907
8. J. Jones, Idaho National Laboratory, Idaho Falls, ID 83415
9. A. W. Hunt, Idaho State University, Pocatello, ID 83209